frontiers in Materials

ORIGINAL RESEARCH
published: 04 February 2020
doi: 10.3389/fmats.2020.00008

Tailoring the Structure, Energy Storage, Strain, and Dielectric Properties of $Bi_{0.5}(Na_{0.82}K_{0.18})_{0.5}TiO_3$ Ceramics by $(Fe_{1/4}Sc_{1/4}Nb_{1/2})^{4+}$ Multiple Complex Ions

Ziwei Huo[1], *Hang Xie*[1], *Jiwen Xu*[1,2*], *Ling Yang*[1], *Wei Qiu*[1], *Xiaowen Zhang*[1,2], *Changrong Zhou*[1,2] *and Hua Wang*[1,2*]

[1] School of Materials Science and Engineering, Guilin University of Electronic Technology, Guilin, China, [2] Guangxi Key Laboratory of Information Materials, Guilin University of Electronic Technology, Guilin, China

OPEN ACCESS

Edited by:
Dawei Wang,
University of Sheffield,
United Kingdom

Reviewed by:
Ruzhong Zuo,
Hefei University of Technology, China
Huiqing Fan,
Northwestern Polytechnical University, China

***Correspondence:**
Jiwen Xu
csuxjw@126.com
Hua Wang
huawang@guet.edu.cn

Specialty section:
This article was submitted to Functional Ceramics, a section of the journal Frontiers in Materials

Received: 25 October 2019
Accepted: 09 January 2020
Published: 04 February 2020

Citation:
Huo Z, Xie H, Xu J, Yang L, Qiu W, Zhang X, Zhou C and Wang H (2020) Tailoring the Structure, Energy Storage, Strain, and Dielectric Properties of $Bi_{0.5}(Na_{0.82}K_{0.18})_{0.5}TiO_3$ Ceramics by $(Fe_{1/4}Sc_{1/4}Nb_{1/2})^{4+}$ Multiple Complex Ions. Front. Mater. 7:8. doi: 10.3389/fmats.2020.00008

The effects of $(Fe_{1/4}Sc_{1/4}Nb_{1/2})^{4+}$ (FSN) multiple complex ions on the structure and electrical properties of $Bi_{0.5}(Na_{0.82}K_{0.18})_{0.5}Ti_{(1-x)}(Fe_{1/4}Sc_{1/4}Nb_{1/2})_xO_3$ (BNKT-*x*FSN) ceramics were studied. The FSN complex ions induce the phase transition from ferroelectric state to relaxor state. The coercive field and remanent polarization decrease rapidly with the increase of FSN content. With the increase of the external electric field, the energy storage density of BNKT-*x*FSN ceramics gradually increases and reaches the maximum value of 0.96 J/cm^3 (90 kV/cm) at $x = 0.09$, and the corresponding efficiency is 62%. Meanwhile, the field-induced strain of BNKT-0.07FSN ceramic increases from 0.13% at 50 kV/cm to 0.43% at 80 kV/cm, and the corresponding electrostrictive coefficient Q_{33} reaches the maximum value of 0.0213 m^4/C^2. BNKT-*x*FSN relaxed ceramics with pseudo-cubic structure have large electrostrictive coefficients when T_d is near room temperature. The local composition inhomogeneity by FSN complex ions at B-sites induces the relaxor characteristics of BNKT-*x*FSN ceramics.

Keywords: BNKT, FSN, complex-ions, energy storage, strain

INTRODUCTION

Lead-free ceramics with ABO_3 perovskite structure are very important part of dielectric materials. Ceramics with perovskite structure are often used in the fields of electronic information, aerospace, defense, and military, and have broad application prospects in the future. It is generally known that pure $Bi_{0.5}Na_{0.5}TiO_3$ (BNT) ceramics are difficult to be practical. However, the modified BNT based ceramics have excellent ferroelectric, piezoelectric and dielectric properties and so on, and are considered to be one of the potential materials to replace lead-based ceramics. By introducing the second phase into the BNT matrix, such as $BaTiO_3$ (BT), $Na_{0.5}Bi_{0.5}TiO_3$ (BKT), the as-formed solid-solution with morphotropic phase boundary (MPB) can be constructed to optimize the structure and properties of BNT-based ceramics (Chen, 2006; Yang et al., 2008; Machado et al., 2016). For example, BNT-BKT solid solution with phases in the vicinity of MPB exhibits excellent electrical properties, such as ferroelectric, dielectric, piezoelectric, strain, and energy storage (Chandrasekhar and Kumar, 2015; Cheng et al., 2015; Li et al., 2015; Guerra et al., 2017; Hajra et al., 2018).

Ion doping as well as solid solution method with ABO_3-type perovskite components (Zou et al., 2010; Zheng and Zuo, 2017; Sui et al., 2019; Zhao et al., 2019) is another common way to modify BNT-based ceramics. Single ion doping substitution is an effective method, such as La^{3+}, Ta^{5+} ions. There are a few works on complex ions doped BNT-based ceramics. However, complex ions doped BNT-based ceramics illustrate excellent electrical properties, such as energy storage, piezoelectric, strain. Zhao et al. obtained a high energy storage density of 1.41 J/cm^3 for BNKT ceramics by the B-site doping of $(Al_{0.5}Nb_{0.5})^{4+}$ complex ions (Zhao et al., 2016). The $(Al_{0.5}Nb_{0.5})^{4+}$ complex ions doped BNT-BT ceramics illustrated high piezoelectric constant of 210 pC/N and large strain response of 0.29% (Hang et al., 2018). Xie et al. doped $(Mg_{1/3}Nb_{2/3})^{4+}$ complex ion into BNKT ceramics, which results in phase change from the ferroelectric phase to ergodic relaxor ferroelectric phase (Xie et al., 2018).

Smolensky et al. first synthesized PMN ferroelectric material with $A(B'_{1/3}B''_{2/3})O_3$ composite perovskite structure (Smolensky et al., 1976). The $A(B'_{1/3}B''_{2/3})O_3$ structure also can be equivalently written as $A[(B'_{2/3}B''_{1/3})_{1/2}B''_{1/2}]O_3$. Therefore, the B-sites of $A[(B'_{2/3}B''_{1/3})_{1/2}B''_{1/2}]O_3$ structure have complex ions, which may illustrates some interesting phenomenon. However, as all we known, these multiple complex ions used for lead-free ceramics has not been reported. Based on the adjustability of structure and properties originating from complex ions, multiple complex ions constructed by three elements are used to modify the B-sites of BNT based ceramics. The B-sites of BNT based ceramics are randomly occupied by as-designed multiple complex ions. The chemical composition inhomogeneity originating from the disorder of ions results in the phase transition and improvement of the electrical properties.

The $(Sc_{1/2}Nb_{1/2})^{4+}$ complex ions were used to modify the phase structure, growth, dielectric and ferroelectric properties of $Pb(Sc_{1/2}Nb_{1/2})_{1-x}Ti_xO_3$ single crystals and ceramics, and $(1-x)Ba(Sc_{1/2}Nb_{1/2})O_3$-$xPbTiO_3$ solid solution (Bing and Ye, 2003; Wei et al., 2009; Tennery et al., 2010). BNT-BKT solid solution doped with $(Fe_{1/2}Nb_{1/2})^{4+}$ complex ions shows high field strain and excellent piezoelectric properties (Fan et al., 2018). Therefore, the Fe^{3+}, Sc^{3+}, and Nb^{5+} ions are selected to construct $(Fe_{1/4}Sc_{1/4}Nb_{1/2})^{4+}$ (FSN) multiple complex ions, which can be equivalently written as $[(Fe_{1/2}Nb_{1/2})_{1/2}(Sc_{1/2}Nb_{1/2})_{1/2}]^{4+}$. The FSN complex ions were used to modify the phase transition, ferroelectric, energy storage, strain, and relaxation properties of BNT-BKT ceramics.

EXPERIMENTAL PROCEDURE

The $Bi_{0.5}(Na_{0.82}K_{0.18})_{0.5}Ti_{1-x}(Fe_{1/4}Sc_{1/4}Nb_{1/2})_xO_3$ (BNKT-xFSN) ceramics with different FNS complex ions contents (x = 0, 0.03, 0.05, 0.07, 0.09, 0.10) were prepared by the solid-state reaction sintering technique. The raw materials of BNKT-xFSN ceramics included high purity oxide powders (Bi_2O_3, Sc_2O_3, Nb_2O_5, Fe_2O_3, TiO_2) and carbonate (K_2CO_3, Na_2CO_3). All of the raw powders were dried at 90°C for at least 1 day, and then weighed according to the stoichiometric formula. The weighed raw powders are mechanically milled by ethanol and zirconium balls for 12 h and then dried at 90°C. The mixed powders were calcinated at 850°C for 2 h to obtain BNKT-xFSN powders. The BNKT-xFSN powders were granulated and added 0.8% polyvinyl alcohol (PVA) as the binder. The 0.35 g granulated powders were pressed at 40 MPa to prepare green body with a diameter of 13 mm. After removing the PVA binder at 600°C for 2 h, The BNKT-xFSN ceramics were sintered at 1,130°C for 2 h. The sintered samples were polished to a thickness of 0.32–0.42 mm. The polished samples were coated with silver electrodes on both sides and fired at 600°C for 0.5 h.

The phase structure of BNKT-xFSN ceramics was analyzed by X-ray diffraction (XRD, D8-Advance, Bruker). The surface morphology of BNKT-xFSN ceramics was analyzed by field emission scanning electron microscopy (FESEM, Quanta 450FEG, FEI). The dielectric properties of BNKT-xFSN ceramics were measured using an impedance analyzer (4294A, Agilent) and a computer-controlled electrical furnace. Ferroelectricity and strain properties were measured by ferroelectric test system (P-PMF, Radiant).

RESULTS AND DISCUSSION

Figure 1A presents the XRD diffraction patterns of BNKT-xFSN ceramics. It can be seen that BNKT-xFSN ceramics show pure perovskite structure with no impurity phases. The FSN complex ions are completely dissolved in the BNKT solid solution and also form a new solid solution. An enlarged view of the (200) peaks in the range of 45∼48° is shown in **Figure 1B**. The (200) peak has no splitting peak, which means that BNKT-xFSN ceramic is a pseudo-cubic phase structure. In addition, the (200) peaks shift to the lower angle with increasing FSN complex ions, which is due to the FNS complex ions with larger average ionic radius (Fe^{3+}: 0.645 Å; Sc^{3+}: 0.745 Å; Nb^{5+}: 0.640 Å) substituting for Ti^{4+} (0.605 Å) ions. This results in the expansion of lattice of BNKT matrix, which is confirmed by the shifting of the (200) diffraction peaks.

Figure 2 shows the surface topography and particle size distribution of BNKT-xFSN ceramics. We can see that the structure of BNKT-xFSN ceramics is dense and has no pores, and the grain boundaries are clear. It can be seen from the particle size distribution that the average grain size of BNKT-xFSN ceramic decreases from 5.91 μm at $x = 0.01$ to 3.04 μm at $x = 0.09$. When the FNS complex ions content is further increased to 0.10, the average grain size hardly increases. Therefore, the FNS complex ions can refine the grains of BNKT ceramics, the average grain size is <6 μm. However, FSN complex ions have no effect on the surface morphology of BNKT-xFSN ceramics.

Figure 3 illustrates the P-E hysteresis loops of BNKT-xFSN ceramics under different electric fields. When $x < 0.07$, it can be seen that the P-E loops are saturated with largely saturated polarization (P_{max}), remnant polarization (P_r) and coercive field (E_c), indicating the typical ferroelectric behavior. At the composition critical point of $x = 0.07$, the pinched P-E hysteresis loops can be obtained, which is similar to double hysteresis loops of anti-ferroelectric. The pinched P-E loops gradually decrease

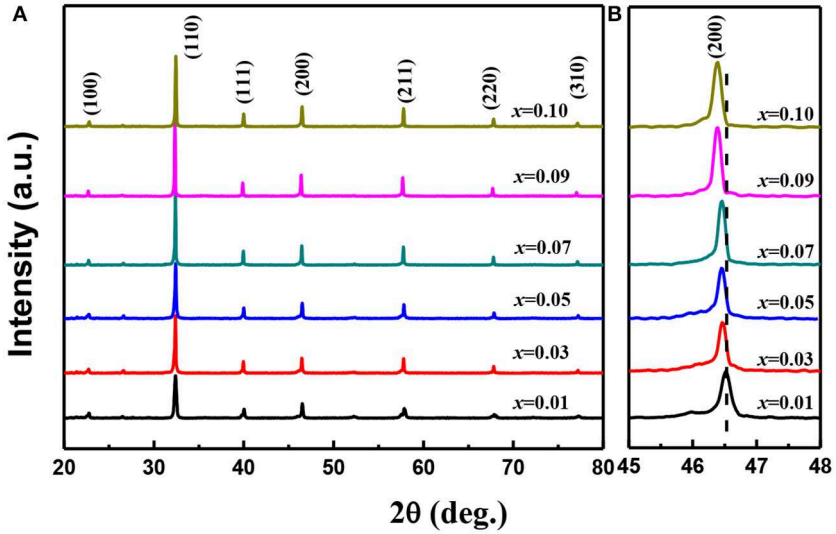

FIGURE 1 | (A) XRD patterns of BNKT-*x*FSN ceramics, **(B)** the magnified view of the (200) peaks.

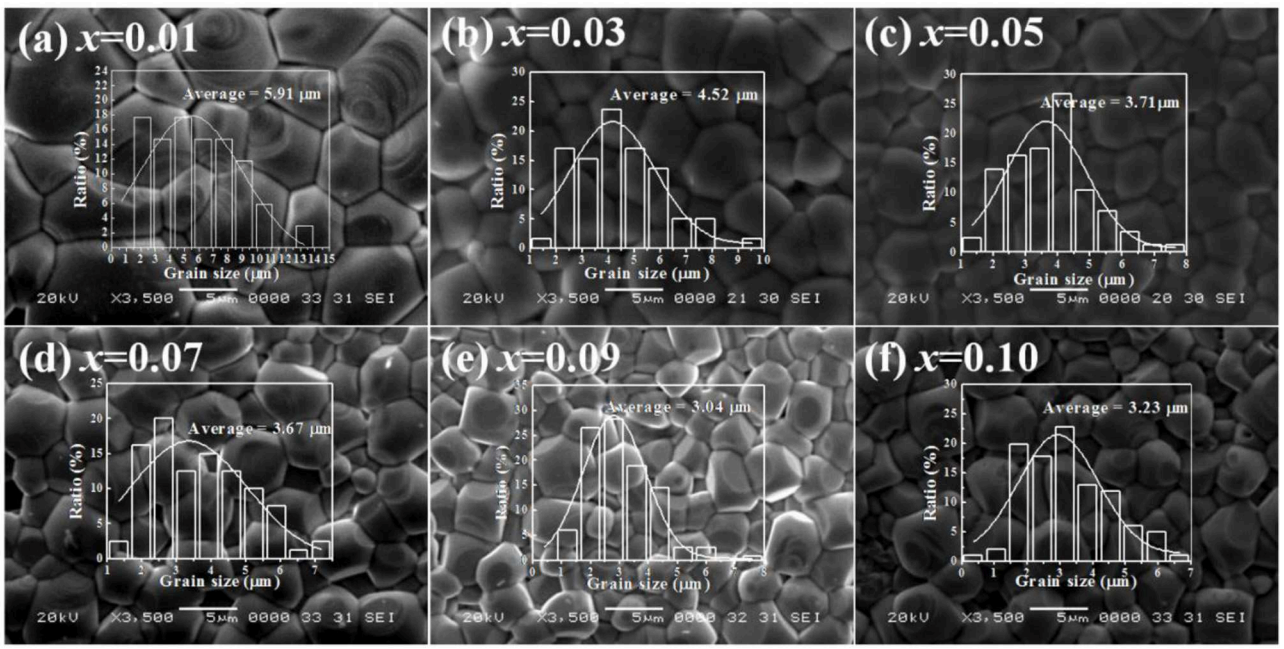

FIGURE 2 | Surface morphology and grain size distribution of BNKT-*x*FSN ceramics with different FSN contents: **(a)** 0.01, **(b)** 0.03, **(c)** 0.05, **(d)** 0.07, **(e)** 0.09, **(f)** 0.10.

the values of P_r and E_c. Further increasing FSN content, the E_c and P_r values almost keep a constant. Therefore, the long-range ordered structure of BNKT-*x*FSN ceramics is destroyed, and the ferroelectric state changes to the relaxor state. This is attributed to the local disturbance of B-sites by $(Fe_{1/4}Sc_{1/4}Nb_{1/2})^{4+}$ complex ions substituting for Ti^{4+} ions. Simultaneously, P_{max} also shows a slight decrease. It is well-known that an excellent energy storage property should have low P_r, high P_{max}, large breakdown strength and double hysteresis loops (Qi and Zuo, 2019). When $x \geq 0.07$, the P_{max} increases almost linearly with the increase of the electric field, while the P_r value hardly changes. At relaxor state with pinched loops, the external electric field promotes the increase of the difference between P_{max} and P_r, which is beneficial to the improvement of energy storage density.

Figure 4 shows the energy storage density and efficiency of BNKT-*x*FSN ceramics under different electric fields. When the FSN content is low, the increase of the electric field has little effect on the energy storage density. When

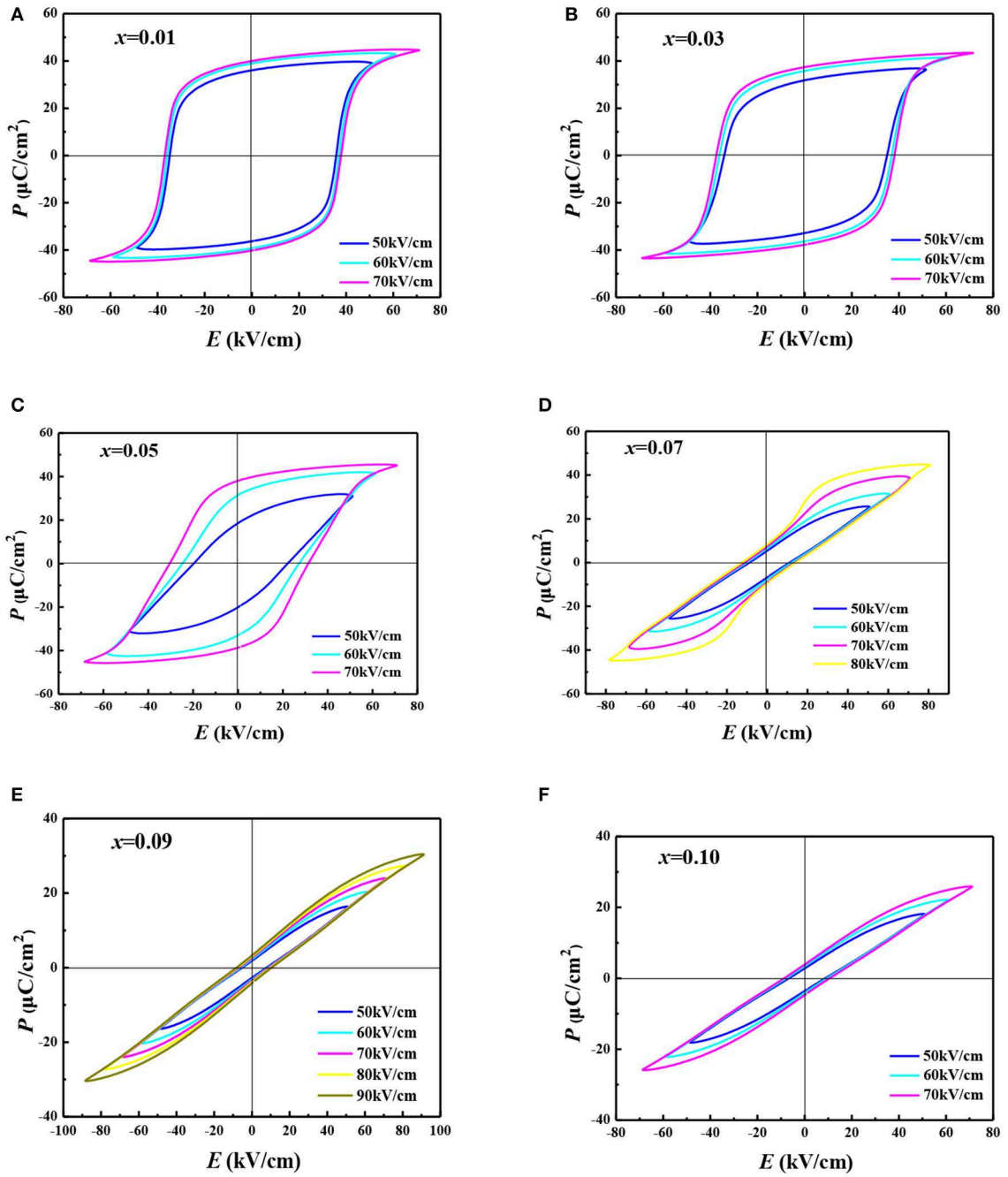

FIGURE 3 | *P-E* loops of BNKT-*x*FSN ceramics under different external electric fields with different FSN contents: **(A)** 0.01, **(B)** 0.03, **(C)** 0.05, **(D)** 0.07, **(E)** 0.09, **(F)** 0.10.

$x \geq 0.07$, the energy storage density increases linearly with the increase of the external electric field. The storage energy density increases from 0.06 J/cm^3 at $x = 0.01$ (50 kV/cm) to 0.96 J/cm^3 at $x = 0.09$ (90 kV/cm). However, the effect of the external electric field on the energy storage efficiency is not obvious. In particular, the high energy storage efficiency is also obtained at $x = 0.09$, which is maintained at about 62%.

Figure 5A shows the *I-E* loops of BNKT-*x*FSN ceramic measured at 70 kV/cm. It can be seen that two current peaks caused by ferroelectric domain switching near E_c illustrate high current intensity when $x = 0.01$ and 0.03. However, there are four current peaks observed from the current curves at $x \geq 0.05$, which indicates that there are two types of polarization switching under the stimulation of the external electric field. The I_2 current peaks represent the ferroelectric-type ($E_{c1} < E_c$) for

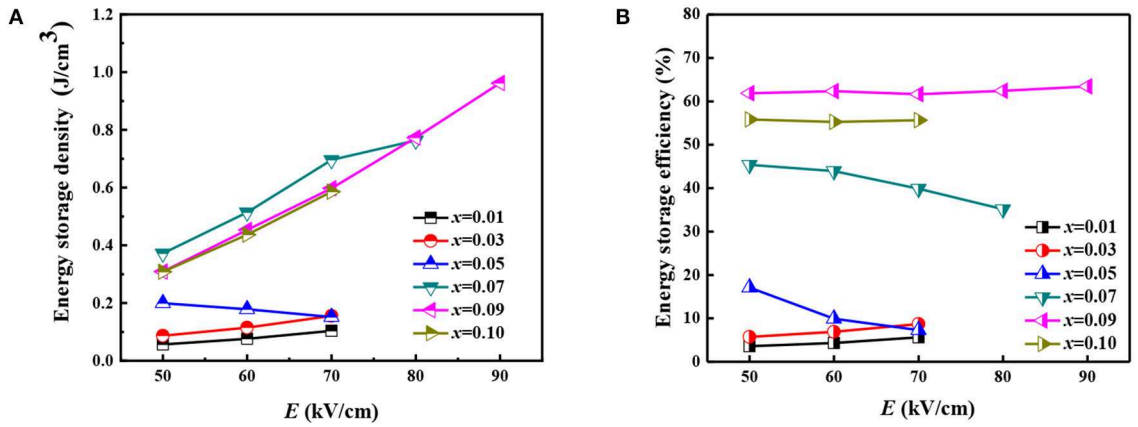

FIGURE 4 | Energy storage **(A)** density and **(B)** Efficiency of BNKT-*x*FSN ceramics under different electric fields.

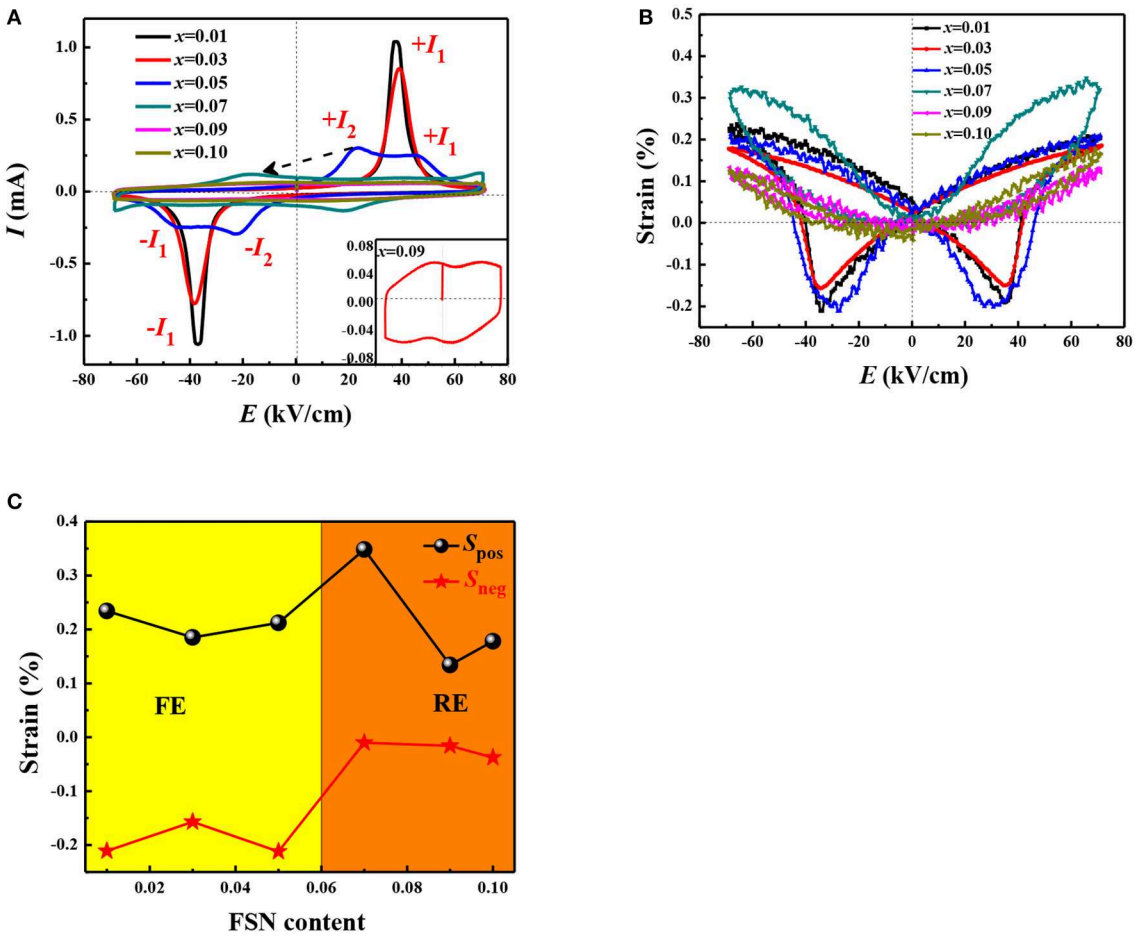

FIGURE 5 | (A) *I-E* loops, **(B)** Bipolar strain loops and **(C)** Positive strain (S_{pos}) and negative strain (S_{neg}) of BNKT-*x*FSN ceramics at 70kV/cm.

the long-range ordered domains being destroyed and forming nanodomains under the external electric field (Guo et al., 2014). This relaxor state gets back to the unstable ferroelectric type with electric field revoked. The I_1 current peaks correspond to the transition process of relaxor-ferroelectric ($E_{c2} > E_c$), which accompanies with the formation and growth of nanodomains

(Jing et al., 2017). The obvious four current peaks at $x = 0.05$ suggest the coexisting of relaxor and the ferroelectric phase (non-ergodic relaxor phase), which is consistent with the results of $(Sr_{1/3}Nb_{2/3})^{4+}$ complex ions doped $0.82Bi_{0.5}Na_{0.5}TiO_3$-$0.18Bi_{0.5}K_{0.5}TiO_3$ ceramics (Zhou et al., 2018). For $x \geq 0.05$, the I_1 and I_2 current peaks shift in opposite directions. The I_1 current peak shift to the high field direction and weakens gradually. However, the I_2 current peaks shift to the zero-electric field, indicating that the induced long-range ferroelectric order will return to relaxor state after removing external electric field (Xing et al., 2016). Ma et al. (2012) proposed by transmission electron microscopy that the four current peaks correspond to the transition between the electric field-induced weakly polarized phase (*P4bm*) and the strongly polarized phase (*R3c* + *P4bm*). In particular, as the doping content increases, the I_2 current peaks gradually shifts to the left and appears in the direction of the reverse electric field. Meanwhile, the current intensity gradually weakens, which indicates that the relaxor behavior is gradually enhanced.

Figure 5B illustrates the bipolar strain loops of BNKT-*x*FSN ceramics at 70 kV/cm. The positive strain (S_{pos}) and negative strain (S_{neg}) under different FSN contents are shown in **Figure 5C**. It can be seen that the bipolar strain curves of BNKT-*x*FSN ceramic at $x < 0.07$ is butterfly-shaped, which corresponds to typical ferroelectricity. With the increase of FSN content, the S_{neg} decreases and tends to zero because the relaxor of BNKT-*x*FSN ceramics is enhanced. Moreover, the shape of strain curves changes from butterfly shape to sprout shape. At $x = 0.07$, the S_{pos} reaches the maximum value of 0.35%. BNKT-*x*FSN ceramics also have a large negative strain at $x = 0.05$, which indicates that the BNKT-*x*FSN ceramic at $x = 0.05$ has strong ferroelectricity, and the transition from the ferroelectric state to relaxor state is in a transitional state. When $x = 0.07$, the negative strain disappears, indicating that the ergodic relaxor phase is the dominated phase, and the field-induced strain reaches the maximum value. When FSN content is further increased, the phase transition is more complete, at which the relaxor state is more stable. Therefore, a larger electric field is required to induce the relaxor-ferroelectric phase transition (Bai et al., 2016).

Figure 6A shows the bipolar strain of BNKT-0.07FSN ceramic under different electric fields. It can be seen that the sprout-shaped strain curves gradually become saturated as the electric

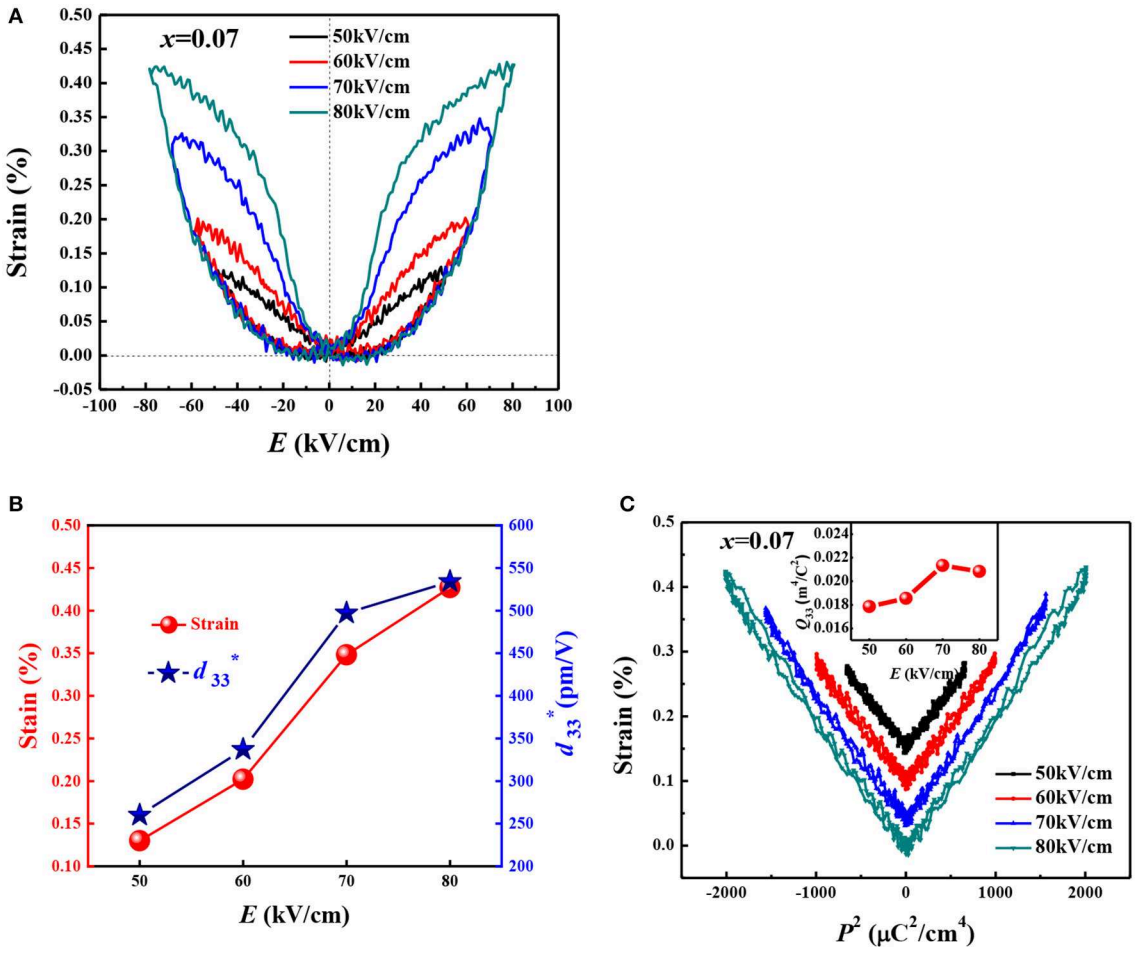

FIGURE 6 | (A) Bipolar strain loops, **(B)** Maximum strain and d_{33}^* and **(C)** *S*-P^2 loops of BNKT-0.07FSN ceramic under different electric fields and the inset shows Q_{33} as the function of different external electric fields.

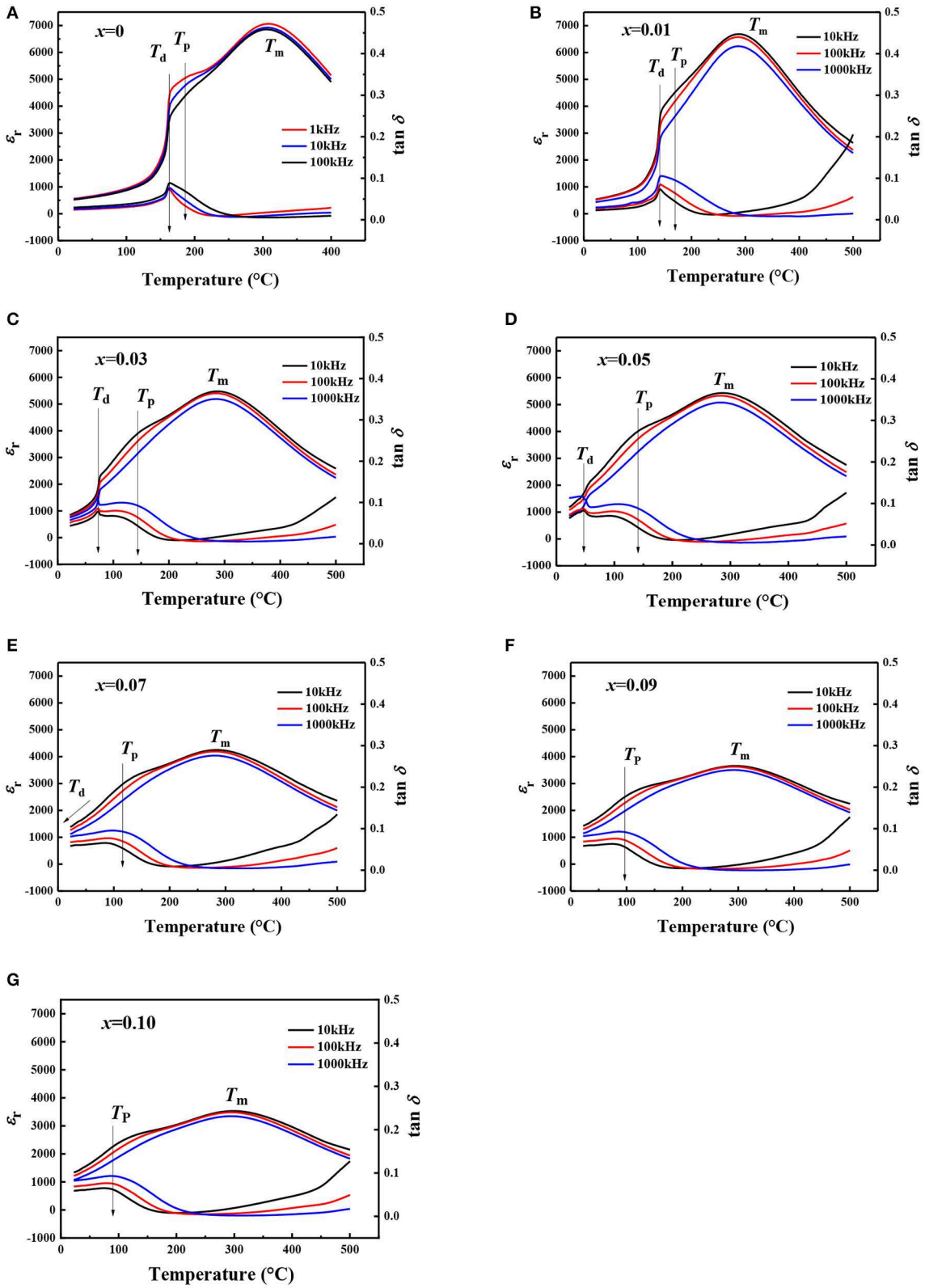

FIGURE 7 | Temperature-dependent dielectric spectra of polarized BNKT-xFSN ceramics with different FSN contents: **(A)** 0, **(B)** 0.01, **(C)** 0.03, **(D)** 0.05, **(E)** 0.07, **(F)** 0.09, **(G)** 0.10.

field increases, and the value of the positive strain increases almost linearly. When the electric field is >60 kV/cm, the positive strain value increases sharply, this further indicates that a larger electric field is required to trigger the relaxor-ferroelectric phase transition. In addition, the field-induced strain has undergone two different stages. For the first stage, BNKT-0.07FSN ceramic remains ergodic relaxor at low field, and the strain mainly comes from the contribution to electrostriction. In the second phase, when the electric field is increased to a certain extent, the strain suddenly increases due to the transition from the ergodic relaxor state to the ferroelectric state. The maximum strain and dynamic piezoelectric constant (d_{33}*) are shown in **Figure 6B**. It can be seen that the maximum positive strain of 0.43% is obtained when the external electric field is increased to 80 kV/cm. The behavior of the corresponding d_{33}* is similar to strain, and the maximum value of 534 pm/V is obtained at 80 kV/cm. In general, piezoelectric effects, electrostriction, and domain wall motion are used to analyze the contribution to field-induced strain behavior. The degree of hysteresis for BNKT-0.07FSN ceramic has a larger value of 53.5%. High electrostrictive strains with low hysteresis for BNT-based ceramics play an important role in precision instrumentation (Bai et al., 2016).

Figure 6C depicts the strain and polarization squared curves of BNKT-0.07FSN ceramics under different electric fields. The electrostrictive coefficient Q_{33} can be obtained by linear fitting of the S-P^2 curve. Analyzed from **Figure 6C**, the S-P^2 curves exhibit a strong linear relationship. As shown in the inset of **Figure 6C**, the electric field has little effect on Q_{33} value, which is similar to the result of BNT-BKT-NN ceramics under different electric fields and temperatures (Bai et al., 2017). At 70 kV/cm, Q_{33} reaches the maximum value of 0.0213 m^4/C^2. Zhang et al. (2010) proposed that the key issue of obtaining high electrostrictive performance for BNT-based relaxor ferroelectric is obtaining pseudocubic phase at room temperature and the depolarization temperature near room temperature or below by adjusting composition. XRD patterns in **Figure 1** indicates that BNKT-0.07FSN composition has a pseudocubic structure at room temperature. Simultaneously, the temperature-dependent dielectric spectra as shown in show **Figures 7A,E** confirm that the depolarization temperature (T_d) of BNKT-xFSN ceramics decreases to room temperature or below. These characteristics meet the above demands, which can explain why BNKT-0.07FSN ceramic has large electrostrictive strain.

Figure 7 shows the temperature-dependent dielectric spectra of the poled BNKT-xFSN ceramics measured from 10 to 1,000 kHz. It can be seen that there are three dielectric anomalies peaks at T_d, T_p, and T_m, as marked in the figures. It can be seen from **Figure 7B** that the first dielectric anomaly peak is located approximately at depolarization temperature T_d (~140°C), which is corresponding to the temperature of the first tanδ peak. It also can be seen from **Figure 7** that T_d decreases below room temperature after $x \geq 0.07$. Some interesting phenomena are observed in BNT-based ceramics at T_d, such as pinched P-E loops, large electric field-induced strain (Zhang et al., 2007; Guo et al., 2011; Xie et al., 2019). The second dielectric anomaly peak occurs at T_p, which is dependent on the measurement frequency. This phenomenon is named as frequency dispersion, which nearly disappears when the frequency increases to 1 MHz. The last dielectric anomaly peak shows at temperature T_m, at which maximal dielectric constant is achieved. The T_m almost keeps constant at around 280°C and the maximum dielectric constant decreases from 6,685 to 3,531 with increasing doping content. We can observe from **Figure 7** that the dielectric peaks at T_m for the samples at $x = 0.07$–0.10 are relatively broad. Jo et al. (2011) proposed the temperature-dependent dielectric behavior of BNT-based ceramics is attributed to the thermal evolution of ferroelectric polar nanoregions of *R3c* and weakly polar *P4bm* symmetry. The broadened T_m peaks and dispersed T_p peaks indicate that BNKT-xFSN ceramics have relaxor behavior. Na^+, K^+, Bi^{3+} occupies A-sites in BNT-based ceramics, and Fe^{3+}, Ti^{4+}, Sc^{3+}, Nb^{5+} occupies B-sites. The difference of ion radius and charge amount form the local field and local elastic field. The local and elastic fields produce PNRs by hindering the long-range ordered dipole moments (Liu et al., 2016). The PNRs leads to the formation of pseudo-cubic structure, which is consistent with the XRD results. The random distribution of A and B-sites cations leads to structural inhomogeneities, which leads to the broadening and dispersion characteristics of the temperature-dependent dielectric spectra.

Based on the above analysis of structure, ferroelectric, strain and dielectric properties, the composition-temperature phase transition of BNKT-xFSN ceramics is summarized as shown in **Figure 8**. It can be seen that T_d drops almost linearly below room temperature, but the T_m maintains almost a constant. At the same time, it can be inferred that the composition between 0.05 and 0.07 is a critical point in which two phases (ferroelectric phase and ergodic relaxor phase) coexist in the BNKT-xFSN ceramics featured by the shifting of T_d to the room temperature. Due to the reduction of energy barriers, the critical component is usually located in a region where polarization reversal and polarization extension mechanisms are strong (Shi et al., 2014). For $x < 0.05$, the ferroelectric phase dominates the phase structure. When $x \geq 0.05$, the ergodic relaxor phase

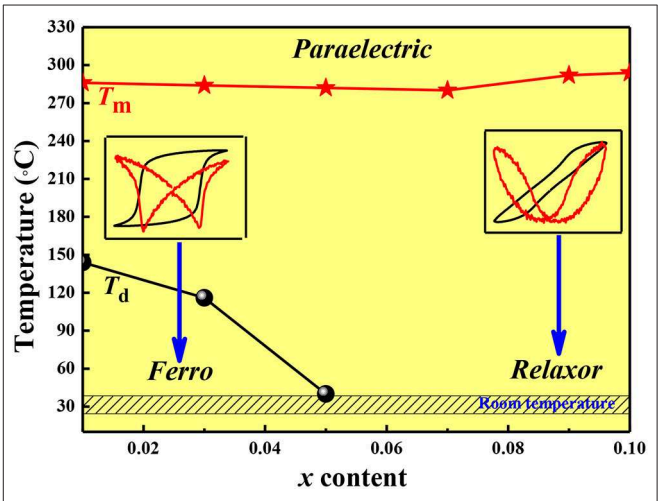

FIGURE 8 | Temperature-composition phase transition diagram of BNKT-xFSN ceramics.

plays a major role. Therefore, the external stimulation, such as doping, temperature, and electric field, can modify the phase transition between the ferroelectric and relaxor states of BNKT-*x*FSN ceramics.

CONCLUSION

The phase, microstructural and electrical properties of $Bi_{0.5}(Na_{0.82}K_{0.18})_{0.5}TiO_3$ ceramics were tailored by $(Fe_{1/4}Sc_{1/4}Nb_{1/2})^{4+}$ multiple complex ions. FSN complex ions doped BNKT ceramics illustrate the pseudo-cubic phase and the expansion of lattice. The grains with uniform size are densely packed together. The surface morphology of grains is independent of FSN content, but grain size decreases gradually. FSN doping induces the phase transition from the ferroelectric state to the relaxor state, which illustrates the decrease of P_r and E_c, and the improvement of energy storage and strain. The maximum energy storage density of 0.96 J/cm^3 is obtained at $x =$ 0.09 and 90 kV/cm, and the corresponding efficiency is 62%. In addition, the strain of BNKT-0.07FSN ceramics increased from 0.13% at 50 kV/cm to 0.43% at 80 kV/cm, and its electrostrictive coefficient reaches the maximum value of 0.0213 m^4/C^2 at 70 kV/cm. The depolarization temperature adjusted by FSN complex ions decrease from 144°C to below room temperature. The B-sites inhomogeneity of BNKT-*x*FSN ceramics induced by FSN multiple complex ions results in the formation of the relaxor characteristics.

DATA AVAILABILITY STATEMENT

All datasets generated for this study are included in the article/supplementary material.

AUTHOR CONTRIBUTIONS

ZH and HX conceived and designed the study. ZH, HX, and WQ performed the experiments. ZH, HW, and JX wrote the paper. LY, XZ, CZ, LY, JX, and HW reviewed and edited the manuscript. All authors read and approved the manuscript.

FUNDING

This work was supported by the National Nature Science Foundation of China (11664006, 61741105, and 61965007). Guangxi Nature Science Foundation (2017GXNSFDA198024 and 2018GXNSFDA281042). Guangxi Key Laboratory of Information Materials (171009-Z) and Innovation Project of GUET Graduate Education (2018YJCX81).

REFERENCES

Bai, W., Chen, D., Huang, Y., Peng, Z., Zhong, J., Ding, M., et al. (2016). Temperature-insensitive large strain response with a low hysteresis behavior in BNT-based ceramics. *Ceram. Int.* 42, 7669–7680. doi: 10.1016/j.ceramint.2016.01.181

Bai, W., Chen, D., Zheng, P., Zhang, J., Shen, B., Zhai, J., et al. (2017). Grain-orientated lead-free BNT-based piezoceramics with giant electrostrictive effect. *Ceram. Int.* 43, 3339–3345. doi: 10.1016/j.ceramint.2016.11.175

Bing, Y. H., and Ye, Z. G. (2003). Effects of chemical compositions on the growth of relaxor ferroelectric $Pb(Sc_{1/2}Nb_{1/2})_{1-x}Ti_xO_3$ single crystals. *J. Cryst. Growth* 250, 118–125. doi: 10.1016/S0022-0248(02)02237-6

Chandrasekhar, M., and Kumar, P. (2015). Synthesis and characterizations of BNT–BT and BNT–BT–KNN ceramics for actuator and energy storage applications. *Ceram. Int.* 41, 5574–5580. doi: 10.1016/j.ceramint.2014.12.136

Chen, Z. (2006). Development of $Bi_{0.5}Na_{0.5}TiO_3$-$BaTiO_3$ and $Bi_{0.5}Na_{0.5}TiO_3$-$Bi_{0.5}K_{0.5}TiO_3$-based lead-free piezoelectric ceramics. *Mater. Rep.* 20, 14—18.

Cheng, R., Xu, Z., Chu, R., Hao, J., Du, J., and Li, G. (2015). Microstructure and electrical properties of $Bi_{1/2}Na_{1/2}TiO_3$-$BaTiO_3$-Y_2NiMnO_6 lead-free piezoelectric ceramics. *Ceram. Int.* 41, 6424–6431. doi: 10.1016/j.ceramint.2015.01.080

Fan, P., Zhang, Y., Xie, B., Zhu, Y., Ma, W., Wang, C., et al. (2018). Large electric-field-induced strain in B-site complex-ion $(Fe_{0.5}Nb0.5)^{4+}$-doped $Bi_{1/2}(Na_{0.82}K_{0.12})_{1/2}TiO_3$ lead-free piezoceramics. *Ceram. Int.* 44, 3211–3217. doi: 10.1016/j.ceramint.2017.11.092

Guerra, J. D. S., Peláiz-Barranco, A., Calderón-Piñar, F., and Mendez-González, Y. (2017). Room temperature antiferroelectric-phase stability in BNT-BT lead-free ceramics. *Phys. Condens. Matter.* 525, 114–118. doi: 10.1016/j.physb.2017.09.014

Guo, Y., Fan, H., and Shi, J. (2014). Origin of the large strain response in tenary $SrTi_{0.8}Zr_{0.2}O_3$ modified $Bi_{0.5}Na_{0.5}TiO_3$-$Bi_{0.5}K_{0.5}TiO_3$ lead-free piezoceramics. *J. Mater. Sci.* 50, 403–411. doi: 10.1007/s10853-014-8599-z

Guo, Y., Gu, M., Luo, H., Liu, Y., and Withers, R. L. (2011). Composition-induced antiferroelectric phase and giant strain in lead-free$(Na_y,Bi_z)Ti_{1-x}O_{3(1-x)}$ $-xBaTiO_3$ ceramics. *Phys. Rev.* 83:054118. doi: 10.1103/PhysRevB.83.054118

Hajra, S., Sahoo, S., Das, R., and R.,Choudhary, N. P. (2018). Structural, dielectric and impedance characteristics of $(Bi_{0.5}Na_{0.5})TiO_3$-$BaTiO_3$ electronic system. *J. Alloys Comp.* 750, 507–514. doi: 10.1016/j.jallcom.2018.04.010

Hang, X., Zhao, Y., Ling, Y., Pang, S., Yuan, C., Hua, W., et al. (2018). Comparative studies on structure, dielectric, strain and energy storage properties of $(Bi_{0.5}Na_{0.5})_{0.94}Ba_{0.06}Ti_{0.965}(Mg_{1/3}Nb_{2/3})_{0.035}O_3$ lead-free ceramics prepared by traditional and two-step sintering method. *J. Mater. Sci. Mater. Electron.* 29, 5349–5355. doi: 10.1007/s10854-017-8500-3

Jing, C., Wang, Y., Zhang, Y., Ying, Y., and Jin, R. (2017). Giant electric field-induced strain at room temperature in $LiNbO_3$-doped $0.94(Bi_{0.5}Na_{0.5})TiO_3$-$0.06BaTiO_3$. *J. Eur. Ceram. Soc.* 37, 2365–2371. doi: 10.1016/j.jeurceramsoc.2017.02.009

Jo, W., Schaab, S., Sapper, E., Schmitt, L. A., Kleebe, H.-J., Bell, A. J., et al. (2011). On the phase identity and its thermal evolution of lead free $(Bi_{1/2}Na_{1/2})TiO_3$-6 mol% $BaTiO_3$. *J. Appl. Phys.* 110:074106. doi: 10.1063/1.3645054

Li, L., Bai, W., Zhang, Y., Shen, B., and Zhai, J. (2015). The preparation and piezoelectric property of textured KNN-based ceramics with plate-like $NaNbO_3$ powders as template. *J. Alloys Comp.* 622, 137–142. doi: 10.1016/j.jallcom.2014.10.014

Liu, G., Fan, H., Dong, G., Shi, J., and Chang, Q. (2016). Enhanced energy storage and dielectric properties of $Bi_{0.487}Na_{0.427}K_{0.06}Ba_{0.026}TiO_3$-$xCeO_2$ anti-ferroelectric ceramics. *J. Alloys Comp.* 664, 632–638. doi: 10.1016/j.jallcom.2015.12.260

Ma, C., Guo, H., Beckman, S. P., and Tan, X. (2012). Creation and destruction of morphotropic phase boundaries through electrical poling: a case study of lead-free $(Bi_{1/2}Na_{1/2})TiO_3$-$BaTiO_3$ piezoelectrics. *Phys. Rev. Lett.* 109:107602. doi: 10.1103/PhysRevLett.109.107602

Machado, R., Ochoa, D. A., dos Santos, V. B., Cerdeiras, E., Mestres, L., and García, J. E. (2016). High stability of properties in morphotropic phase boundary $Bi_{0.5}Na_{0.5}TiO_3$-$BaTiO_3$ piezoceramics. *Mater. Lett.* 183, 73–76. doi: 10.1016/j.matlet.2016.07.045

Qi, H., and Zuo, R. (2019). Linear-like lead-free relaxor antiferroelectric $(Bi_{0.5}Na_{0.5})TiO_3$-$NaNbO_3$ with giant energy-storage density/efficiency and super stability against temperature and frequency. *J. Mater. Chem. A* 7, 3971–3978. doi: 10.1039/C8TA12232F

Shi, J., Fan, H., Liu, X., and Li, Q. (2014). Giant strain response and structure evolution in $(Bi_{0.5}Na_{0.5})_{0.945-x}(Bi_{0.2}Sr_{0.7}\square_{0.1})_xBa_{0.055}TiO_3$ ceramics. *J. Eur. Ceram. Soc.* 34, 3675–3683. doi: 10.1016/j.jeurceramsoc.2014.05.032

Smolensky, G. A., Siny, I. G., Pisarev, R. V., and Kuzminov, E. G. (1976). Raman scattering in ordered and disordered perovskite type crystals. *Ferroelectrics.* 12, 135–136. doi: 10.1080/00150197608241407

Sui, J., Fan, H., Peng, H., Ma, J., Yadav, A. K., Chao, W., et al. (2019). Enhanced energy-storage performance and temperature-stable dielectric properties of $(1–x)[(Na_{0.5}Bi_{0.5})0.95Ba_{0.05}]_{0.98}La_{0.02}TiO_3$-$xK_{0.5}Na_{0.5}NbO_3$ lead-free ceramics. *Ceram. Int.* 45, 20427–20434. doi: 10.1016/j.ceramint.2019.07.019

Tennery, V. J., Hang, K. W., and Novak, R. E. (2010). Ferroelectric and structural properties of the $Pb(Sc_{1/2}Nb_{1/2})_{1-\infty}$-$Ti_\infty O_3$ system. *J. Am. Ceram. Soc.* 51, 671–674. doi: 10.1111/j.1151-2916.1968.tb15925.x

Wei, Q., Wang, Z., Li, X., Long, X., and Z.-,Ye, G. (2009). Morphotropic phase diagram and dielectric and ferroelectric properties of $(1–x)Ba(Sc_{1/2}Nb1_{/2})O_3$-$x$PbTiO$_3$ solid solution. *Chem. Mater.* 21, 506–510. doi: 10.1021/cm802734n

Xie, H., Yang, L., Pang, S., Yuan, C., Chen, G., Wang, H., et al. (2019). The evolution of phase structure, dielectric, strain, and energy storage density of complex-ions $(Sr_{1/3}Nb_{2/3})^{4+}$ doped $0.82Bi_{0.5}Na_{0.5}TiO_3$-$0.18Bi_{0.5}K_{0.5}TiO_3$ ceramics. *J. Phys. Chem. Solids* 126, 287–293. doi: 10.1016/j.jpcs.2018.11.030

Xie, H., Zhao, Y., Xu, J., Yang, L., Zhou, C., Zhang, H., et al. (2018). Structure, dielectric, ferroelectric, and field-induced strain response properties of $(Mg_{1/3}Nb_{2/3})^{4+}$ complex-ion modified $Bi_{0.5}(Na_{0.82}K_{0.18})_{0.5}TiO_3$ lead-free ceramics. *J. Alloys Comp.* 743, 73–82. doi: 10.1016/j.jallcom.2018.01.367

Xing, L., Zhai, J., Bo, S., Feng, L., Yang, Z., Peng, L., et al. (2016). Electric-field-temperature phase diagram and electromechanical properties in lead-free $(Na_{0.5}Bi_{0.5})TiO_3$-based incipient piezoelectric ceramics. *J. Eur. Ceram. Soc.* 37, 1437–1447. doi: 10.1016/j.jeurceramsoc.2016.12.020

Yang, Z., Liu, B., Wei, L., and Hou, Y. (2008). Structure and electrical properties of $(1–x)Bi_{0.5}Na_{0.5}TiO_3$-$xBi_{0.5}K_{0.5}TiO_3$ ceramics near morphotropic phase boundary. *Mater. Res. Bull.* 43, 81–89. doi: 10.1016/j.materresbull.2007.02.016

Zhang, S. T., Kounga, A. B., Aulbach, E., Ehrenberg, H., and Rödel, J. (2007). Giant strain in lead-free piezoceramics $Bi_{0.5}Na_{0.5}TiO_3$-$BaTiO_3$-$K_{0.5}Na_{0.5}NbO_3$ system. *Appl. Phys. Lett.* 91:112906. doi: 10.1063/1.2783200

Zhang, S. T., Yan, F., Yang, B., and Cao, W. (2010). Phase diagram and electrostrictive properties of $Bi_{0.5}Na_{0.5}TiO_3$-$BaTiO_3$-$K_{0.5}Na_{0.5}NbO_3$ ceramics. *Appl. Phys. Lett.* 97:122901. doi: 10.1063/1.3491839

Zhao, N., Fan, H., Ren, X., Ma, J., Bao, J., Guo, Y., et al. (2019). Dielectric, impedance and piezoelectric properties of $(K_{0.5}Nd_{0.5})TiO_3$-doped $0.67BiFeO_3$-$0.33BaTiO_3$ ceramics. *J. Eur. Ceram. Soc.* 39, 4096–4102. doi: 10.1016/j.jeurceramsoc.2019.06.001

Zhao, Y., Xu, J., Yang, L., Zhou, C., Lu, X., Yuan, C., et al. (2016). High energy storage property and breakdown strength of $Bi_{0.5}(Na_{0.82}K_{0.18})_{0.5}TiO_3$ ceramics modified by $(Al_{0.5}Nb_{0.5})^{4+}$ complex-ion. *J. Alloys Comp.* 666, 209–216. doi: 10.1016/j.jallcom.2016.01.103

Zheng, D., and Zuo, R. (2017). Enhanced energy storage properties in $La(Mg_{1/2}Ti_{1/2})O_3$-modified $BiFeO_3$-$BaTiO_3$ lead-free relaxor ferroelectric ceramics within a wide temperature range. *J. Eur. Ceram. Soc.* 37, 413–418. doi: 10.1016/j.jeurceramsoc.2016.08.021

Zhou, C., Li, Q., Xu, J., Ling, Y., Zeng, W., Yuan, C., et al. (2018). Ferroelectric-quasiferroelectric-ergodic relaxor transition and multifunctional electrical properties in $Bi_{0.5}Na_{0.5}TiO_3$-based ceramics. *J. Am. Ceram. Soc.* 101, 1554–1565. doi: 10.1111/jace.15308

Zou, M., Fan, H., Chen, L., and Yang, W. (2010). Microstructure and electrical properties of $(1–x)[0.82Bi_{0.5}Na_{0.5}TiO_3$-$0.18Bi_{0.5}K_{0.5}TiO_3]–xBiFeO_3$ lead-free piezoelectric ceramics. *J. Alloys Comp.* 495, 280–283. doi: 10.1016/j.jallcom.2010.02.025

Conflict of Interest: The authors declare that the research was conducted in the absence of any commercial or financial relationships that could be construed as a potential conflict of interest.